Atomic-beam measurement of parity nonconservation in cesium

S. L. Gilbert* and C. E. Wieman

*Joint Institute for Laboratory Astrophysics, University of Colorado and National Bureau of Standards,
Campus Box 440, Boulder, Colorado 80309-0440
and Physics Department, University of Colorado, Boulder, Colorado 80309-0440*

We present a new measurement of parity nonconservation in cesium. In this experiment, a laser excited the $6S \rightarrow 7S$ transition in an atomic beam in a region of static electric and magnetic fields. The quantity measured was the component of the transition rate arising from the interference between the parity nonconserving amplitude, $\mathscr{E}_{PNC}$, and the Stark amplitude, βE. Our results are $\text{Im}\mathscr{E}_{PNC}/\beta = -1.65 \pm 0.13$ mV/cm and $C_{2p} = -2 \pm 2$, where C_{2p} is the proton-axial-vector—electron-vector neutral-current coupling constant. These results are in agreement with previous less precise measurements in cesium and with the predictions of the electroweak standard model. We give a detailed discussion of the experiment with particular emphasis on the treatment and elimination of systematic errors. This experimental technique will allow future measurements of significantly higher precision.

I. INTRODUCTION

The standard model of electroweak unification has stimulated considerable interest in atomic parity nonconservation (PNC) over the last decade. This theory predicted a PNC neutral-current interaction between electrons and nucleons which would mix the parity eigenstates of an atom. Although the standard model has now been tested with moderate precision in a variety of experiments using high-energy accelerators, atomic PNC data can provide unique and complementary information about this interaction. This is because the atomic case probes a very different energy scale and is sensitive to a different set of electron-quark coupling constants. Thus precise atomic data would allow one to measure the radiative corrections[1] to the electroweak theory and to explore the possible alternatives to the standard model over a larger parameter space.

In pursuit of this goal, measurements of parity nonconservation have now been carried out on bismuth,[2] lead,[3] thallium,[4] and cesium.[5,6] The approximately Z^3 dependence of the PNC mixing is the reason for the emphasis on high-Z atoms. Aside from some ambiguity in the early bismuth results, all of the data are now in agreement with the predictions of the standard model. While this work has provided significant new information, its importance has been limited by two factors. The first has been the level of precision of the experimental results, and the second is the difficulty in relating the observations to the fundamental electron-nucleon interaction because of the complexities of the atomic structure.

To overcome these limitations we have developed a new experimental technique which will allow precise measurements on cesium. Cesium has the virtue that it is the simplest heavy atom, having one S-state electron outside a filled inner core. Thus it is highly single-electron in character and calculations of its structure are more direct and accurate than for other heavy atoms. In addition, there is

a wealth of precise experimental data on the various properties of cesium ground and excited states which can be used for testing and refining calculations of its wave functions.

In a previous paper[6] we briefly presented the results of our first measurement using this new technique. Although we expect considerable future improvement, this measurement is already more precise than previous measurements of atomic PNC and is approaching the pre-
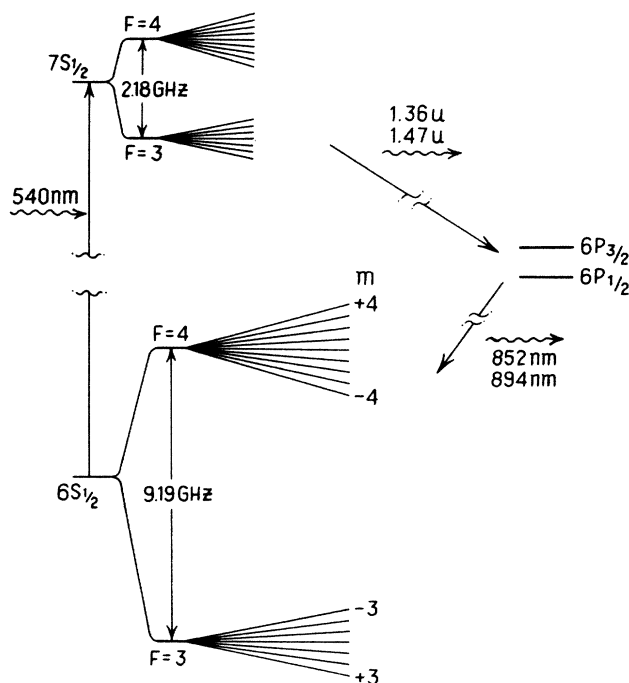
FIG. 1. Cesium-energy-level diagram showing hyperfine and weak-field Zeeman structure of the $6S$ and $7S$ states.

cision of the best high-energy tests of the electroweak theory. Here we give a detailed discussion of this experiment with particular emphasis on the critical issue of the treatment and elimination of systematic errors.

The PNC interaction in an atom mixes S and P eigenstates, allowing a small electric dipole ($E1$) transition amplitude between states of the same parity. Similar to all atomic PNC experiments, we measure this small parity nonconserving amplitude (A_{PNC}) by observing its interference with a larger parity conserving amplitude. In our experiment, the parity conserving amplitude is a "Stark induced" $E1$ amplitude (A_{ST}) created by applying a dc electric field to mix S and P states. The use of this amplitude was first suggested by the Bouchiats[7] and it was used in the cell experiments discussed in Refs. 4 and 5. In our experiment we use a laser to excite the transition of interest in an atomic beam. The use of an atomic beam nearly eliminates the Doppler broadening and hence we obtain very narrow transition lindwidths. This enables us to observe the PNC interference directly in the transition rate by applying a small magnetic field (70 G) to break the degeneracy of the Zeeman levels.[8] Other advantages of an atomic-beam experiment include the reduction of collisions, radiation trapping, and molecular backgrounds. A final important feature of our approach is that the transitions can be detected with high efficiency.

In this paper we will first discuss the theory of the experiment in Sec. II. In Sec. III we will discuss the apparatus and experimental procedure and in Sec. IV we cover the treatment of systematic errors. In Sec. V we present the results and in Sec. VI discuss the future improvements to the experiment.

II. THEORY

In this section we present the basic theory needed to understand and interpret the experiment. We are interested in the excitation of the $6S$ state of cesium to the $7S$ state by a resonant electromagnetic field in the presence of static electric and magnetic fields. This problem has been previously discussed for the case of large magnetic fields and broad transition linewidths.[9] Here we consider the case of narrow linewidths and a weak magnetic field which has a relatively simple analytic solution. There are three relevant transition amplitudes which can give rise to this excitation; a Stark induced electric dipole, a magnetic dipole, and the PNC electric dipole. We will first consider the total transition amplitude between a particular ground state ($6S,F,m$) and excited state ($7S,F',m'$) level, where m (m') is the z component of the total angular momentum F (F'). This derivation applies to the general case of arbitrary dc electric and laser field orientations. Combining this result for the amplitude with knowledge of how the Zeeman levels shift in a weak magnetic field, we will then derive the transition spectrum for the particular field configuration we have chosen.

Figure 1 is the cesium-energy-level diagram for the transitions of interest in this experiment. With a static electric field, E, and an oscillating (laser) electric field, ε, the Stark-induced transition amplitude between the perturbed $6S(F,m)$ and $7S(F',m')$ states is

$$A_{ST}(F,m;F',m') = \langle \overline{7S,F',m'} \mid -\mathbf{d}\cdot\varepsilon \mid \overline{6S,F,m} \rangle$$

$$= [\alpha \mathbf{E}\cdot\varepsilon\delta_{F,F'} + i\beta(\mathbf{E}\times\varepsilon)_z C_{Fm}^{F'm'}]\delta_{m,m'} + [\pm i\beta(\mathbf{E}\times\varepsilon)_x - \beta(\mathbf{E}\times\varepsilon)_y]C_{Fm}^{F'm'}\delta_{m,m'\pm 1}, \tag{1}$$

where $\mathbf{d}$ is the electric dipole operator. The coefficients $C_{Fm}^{F'm'}$ are proportional to the usual Clebsch-Gordan coefficients and are tabulated in Appendix A. The quantities α and β are the scalar and vector transition polarizabilities respectively and are given by[7]

$$\alpha = \frac{1}{6}\sum_n \left[\langle 7S||r||nP_{1/2}\rangle\langle nP_{1/2}||r||6S\rangle \left[\frac{1}{E_{7S}-E_{nP_{1/2}}} + \frac{1}{E_{6S}-E_{nP_{1/2}}} \right] \right.$$

$$\left. - \langle 7S||r||nP_{3/2}\rangle\langle nP_{3/2}||r||6S\rangle \left[\frac{1}{E_{7S}-E_{nP_{3/2}}} + \frac{1}{E_{6S}-E_{nP_{3/2}}} \right] \right],$$

$$\beta = \frac{1}{6}\sum_n \left[\langle 7S||r||nP_{1/2}\rangle\langle nP_{1/2}||r||6S\rangle \left[\frac{1}{E_{7S}-E_{nP_{1/2}}} - \frac{1}{E_{6S}-E_{nP_{1/2}}} \right] \right.$$

$$\left. + \frac{1}{2}\langle 7S||r||nP_{3/2}\rangle\langle nP_{3/2}||r||6S\rangle \left[\frac{1}{E_{7S}-E_{nP_{3/2}}} - \frac{1}{E_{6S}-E_{nP_{3/2}}} \right] \right].$$

$$\tag{2}$$

Similarly, the magnetic dipole transition amplitude between these states is

$$A_{M1}(F,m;F',m') = \{(\hat{\mathbf{k}}\times\varepsilon)_z\delta_{m,m'} + [\pm(\hat{\mathbf{k}}\times\varepsilon)_x + i(\hat{\mathbf{k}}\times\varepsilon)_y]\delta_{m,m'\pm 1}\}MC_{Fm}^{F'm'} \tag{3}$$

where $\mathbf{k}$ is the laser propagation vector. M is the highly forbidden magnetic dipole ($M1$) matrix element defined as

$$M = \langle 7S \mid \mu_z/c \mid 6S \rangle, \tag{4}$$

where μ_z is the z component of the magnetic dipole operator. The parity nonconserving potential, V_{PNC}, mixes S and P states and gives rise to a transition amplitude given by

$$A_{\text{PNC}}(F,m,F',m') = [\varepsilon_z \delta_{m,m'} + (\pm \varepsilon_x + i\varepsilon_y)\delta_{m,m'\pm 1}]i \, \text{Im} \mathscr{E}_{\text{PNC}} C_{Fm}^{F'm'} . \tag{5}$$

$\mathscr{E}_{\text{PNC}}$ is the parity-nonconserving matrix element defined by Bouchiat and Bouchiat[7] as

$$\mathscr{E}_{\text{PNC}} = \langle 7S \mid d_z \mid 6S \rangle$$

$$= \sum_{nP} \left[\frac{\langle 7S \mid V_{\text{PNC}} \mid nP \rangle \langle nP \mid d_z \mid 6S \rangle}{E_{7S} - E_{nP}} + \frac{\langle 7S \mid d_z \mid nP \rangle \langle nP \mid V_{\text{PNC}} \mid 6S \rangle}{E_{6S} - E_{nP}} \right] . \tag{6}$$

Combining all three transition amplitudes, the transition probability between particular sublevels (m and m') is then

$$I = |A_{\text{ST}} + A_{M1} + A_{\text{PNC}}|^2 \tag{7}$$

where each A is a function of F, F', m, and m'.

We chose the experimental design to maximize the interference between A_{ST} and A_{PNC} while minimizing the $A_{\text{ST}} - A_{M1}$ interference and other effects which may mimic the PNC signal. It should be noted that the PNC interference term is dependent on m. If the m levels are degenerate and equally populated this term will sum to zero in the total rate for the $F \rightarrow F'$ transition. A magnetic field is introduced to break the degeneracy of the m levels and hence avoid this cancellation. The field configuration used[10] is shown in Fig. 2. A standing wave laser beam along the $\hat{y}$ axis excites transitions in a region of dc electric field in the $\hat{x}$ direction and dc magnetic field ($\mathbf{B}$) along the $\hat{z}$ axis. The laser field is elliptically polarized with $\varepsilon = \varepsilon_z \hat{z} + i\varepsilon_x \hat{x}$ where ε_x and ε_z are real. Using this field configuration and substituting the amplitudes from Eqs. (1), (3), and (5) into Eq. (7), we obtain for $F \neq F'$,

$$I_{Fm}^{F'm'} = [\beta^2 E^2 \varepsilon_z^2 \mp 2\beta E \varepsilon_z \, \text{Im} \mathscr{E}_{\text{PNC}} \varepsilon_x$$

$$\pm 2\beta EM (\mid \varepsilon_z^{k+} \mid^2 - \mid \varepsilon_z^{k-} \mid^2)](C_{Fm}^{F'm'})^2 \delta_{m,m'\pm 1} \tag{8}$$

plus negligibly small terms involving only $\mathscr{E}_{\text{PNC}}$ and M. The quantities ε_z^{k+} and ε_z^{k-} represent the z components of the laser field for the $\hat{k} = +\hat{y}$ and $\hat{k} = -\hat{y}$ laser beam propagation directions respectively, and $\varepsilon_z^2 = \mid \varepsilon_z^{k+} + \varepsilon_z^{k-} \mid^2$. The first term in Eq. (8) is the pure Stark-induced transition rate and the second term is the interference between A_{ST} and the much smaller amplitude A_{PNC}. This corresponds to the pseudoscalar $\xi \hat{k} \cdot \mathbf{E} \times \mathbf{B}$

where ξ represents the handedness of the laser polarization. The third term is the interference between A_{ST} and A_{M1}. For our standing-wave laser field, $\varepsilon_z^{k+} \approx \varepsilon_z^{k-}$, which leads to a cancellation of the $A_{\text{ST}} - A_{M1}$ interference. The problem of imperfect cancellation of this term and other effects due to imperfect ε, $\mathbf{E}$, and $\mathbf{B}$ fields will be addressed in Sec. IV.

In the weak magnetic field limit, each Zeeman sublevel is shifted in frequency by an amount $\Delta \nu = mg_F \mu_B B$, where $g_{F=4} = -g_{F=3} = \frac{1}{4}$ for S states. Applying this to the field configuration of our experiment, we find the spectrum of the $6S(F=4) \rightarrow 7S(F=3)$ transition to be composed of eight lines with strengths, $R(i)$, given by

$$R(i) = I_{4,i-1}^{3,i} + I_{4,i}^{3,i-1}, \quad i = -3, -2, \ldots, +4 . \tag{9}$$

The two outermost lines of the multiplet involve only a single Zeeman transition ($m = 4 \rightarrow 3$ and $m = -4 \rightarrow -3$, respectively) while the other lines are each the sum of a $\Delta m = +1$ and a $\Delta m = -1$ transition. The $F = 4 \rightarrow 3$ spectrum is shown in Fig. 3 where the transition rate for each line is the sum of contributions (a) and (b). In the weak-field limit, the spectrum for the $F = 3 \rightarrow 4$ transition is identical.

These spectra are modified slightly due to magnetic

FIG. 2. Field configuration for experiment.
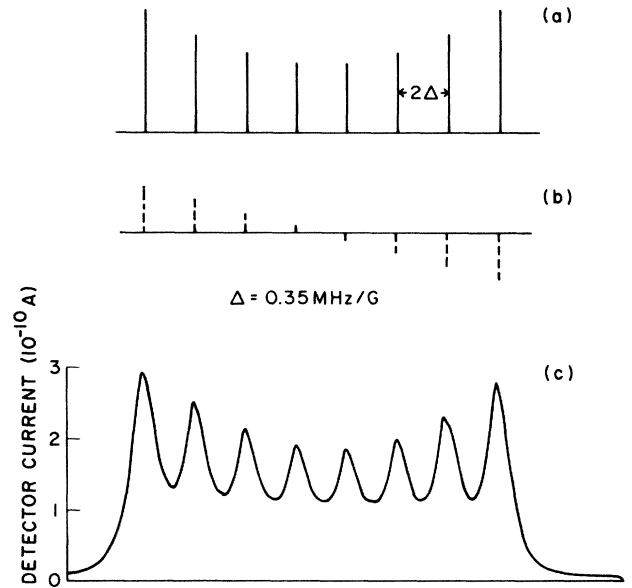
FIG. 3. $6S_{F=4} \rightarrow 7S_{F=3}$ transition. (a) Theoretical pure Stark-induced spectrum. (b) Theoretical parity nonconserving interference spectrum on expanded scale. (c) Experimental scan of the transition with $B = 70$ G.

field induced mixing of hyperfine states. This causes the right-left asymmetry of the peak heights in Fig. 3(c), for example. However, the mixing is quite small and can be accurately calculated using first-order perturbation theory. We calculate that a 70 G magnetic field causes the extreme left- and right-hand peak heights of the $F = 4 \rightarrow 3$ transition to differ by about 5%. The asymmetry is smaller on the $F = 3 \rightarrow 4$ transition by the ratio of the $7S$ to $6S$ hyperfine splittings (~ 0.25). The magnetic field induced mixing, however, is not important in our experiment because we only make measurements on the two outermost lines of the multiplet where the A_{ST} and A_{PNC} contributions are affected equally. Thus the ratio A_{PNC}/A_{ST}, which is the quantity of interest, is independent of this mixing.

III. EXPERIMENT

A laser, tuned to one of the end lines of the multiplet shown in Fig. 3, excited the $6S \rightarrow 7S$ transition in cesium. We monitored the transition rate by measuring the amount of 850- and 890-nm light emitted in the $6P_{1/2,3/2} \rightarrow 6S$ step of the $7S \rightarrow 6P \rightarrow 6S$ decay sequence. The essence of the experiment can be understood from Eq. (8) and Fig. 3. The parity nonconserving interference term in Eq. (8) changes sign under the reversal of the E field, the B field, and the sign of ε_x (handedness of laser polarization). This causes a slight change in the overall transition rate, and hence provides a means of isolating the PNC interference term from the much larger pure Stark-induced term. An additional reversal ("m" reversal) was achieved by changing the laser frequency to the other end of the multiplet. We have used this technique to measure the ratio of the PNC amplitude to the Stark-induced amplitude for the $6S(F=4) \rightarrow 7S(F=3)$ and $6S(F=3) \rightarrow 7S(F=4)$ transitions.

A. Apparatus

The basic experimental setup is shown in Fig. 4. Laser light at 540 nm was produced by a dye laser and the beam passed through several optical elements before entering a vacuum chamber. Inside the vacuum chamber the laser beam was coupled into a Fabry-Perot interferometer, referred to as the power-buildup cavity (PBC) in Fig. 4. The PBC was maintained in reasonance with the laser which resulted in a large standing wave field inside the cavity. This field induced transitions in a cesium beam in
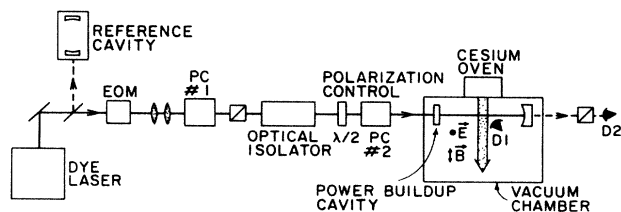
FIG. 4. Schematic of apparatus. PC no. 1 and PC no. 2 are the intensity stabilization and polarization control Pockels cells, respectively. $D1$ is the transition detector (actually situated below the cesium beam) and $D2$ is the PBC transmission detector.

a region of static electric and magnetic fields. A silicon photodiode detected the fluorescence emitted by the decay of the excited state. In the following paragraphs, we will discuss each of the key elements of the apparatus.

A Spectra-Physics Model No. 380 ring dye laser produced approximately 500 mW of light at 540 nm. We found it necessary to reduce the frequency fluctuations of the laser. To accomplish this, a few percent of the laser output power was sent to a stable reference interferometer cavity and an error signal was derived from the cavity reflection using the Hänsch-Couillaud method.[11] The error signal was used to control the galvanometer driven plates and a piezoelectric transducer (PZT) mounted mirror in the dye-laser cavity. This reduced the laser linewidth to about 100 kHz. A Brewster angle galvanometer driven plate within the reference interferometer allowed cavity optical length adjustment. This in turn produced laser frequency tuning when the laser was locked to the reference cavity. As will be discussed below, the long-term stability of the reference cavity was insured by locking it to the cesium transition frequency.

The main laser beam passed through many optical elements. The first element was an electro-optic modulator (EOM) which produced small 4-MHz frequency-modulation (FM) sidebands on the laser. As discussed below, this was necessary for the scheme which we used to hold the power-buildup cavity in resonance. Following the electro-optic modulator, two lenses modematched the laser into the lowest-order spatial mode of the PBC. The next element was a Pockels cell which, in combination with a linear polarizer, enabled stabilization of the laser intensity with active feedback. Following the intensity stabilization Pockels cell, the laser passed through a Faraday rotation optical isolator which isolated the laser from reflected beams. At the output of the optical isolator, the laser light was linearly polarized at 45° with respect to the $\hat{x}$ axis defined in Fig. 2.

The next component in the laser beam path was the polarization control element which set the ellipticity and handedness of the laser polarization. The polarization control element was made up of a $\lambda/2$ retardation plate followed by a longitudinal single-crystal [potassium dihydrogen phosphate (KDP)] Pockels cell. When 1.85 kV was applied, the Pockels cell produced a $\lambda/4$ (90°) phase retardation on the x component of the laser field. We adjusted the ellipticity of the light by rotating the (linear) laser polarization at the input of the Pockels cell with the $\lambda/2$ plate. The handedness of the laser polarization was then changed by reversing the voltage applied to the Pockels cell ($+\lambda/4 \rightarrow -\lambda/4$ retardation). We reversed this voltage using a double-pole double-throw vacuum relay. The Pockels cell had a 1-cm aperture and provided quite uniform birefringence across the 0.05-cm-diameter laser beam. It was necessary to temperature stabilize the Pockels cell and isolate it from air currents to minimize variations in the resultant laser polarization. With these precautions, the birefringence of the Pockels cell was stable to a few parts in 10^5 over the course of an 8-h data run.

Following the polarization control element, the laser beam entered the vacuum chamber (pressure 3×10^{-7} Torr) and was coupled into the power-buildup cavity.

The PBC was a spherical mirror Fabry-Perot interferometer with a mirror separation of 23 cm. The flat, partially transmitting ($R = 98.5\%$ and $T = 1.3\%$) input mirror was mounted on a piezo-electric transducer. The second mirror had a reflectivity of 99.8% and a 50-cm radius of curvature. The power-buildup cavity was maintained in resonance with the laser using the FM sideband stabilization technique.[12] We implemented this by using a fast photodiode to detect the laser beam which was reflected off the PBC. The output of the photodiode went to a phase-sensitive demodulator operating at the EOM 4-MHz drive frequency. This produced an error signal which was then fed to the PZT mounted input mirror of the power-buildup cavity.

When locked on resonance, the laser field within the power-buildup cavity was 20 times that of the incident laser beam. We monitored the power in the PBC by detecting the light which was transmitted through the second PBC mirror. The intensity at this detector was held constant to better than one part in 10^5 per sec$^{1/2}$ by a feedback loop which controlled the intensity stabilization Pockels cell. We found that our signal-to-noise ratio was improved by about a factor of 2 by inserting a linear polarizer with its axis along the z direction in front of this detector. This means that we were only stabilizing the intensity of the field component (ε_z) which drove the pure Stark-induced term in Eq. (8).

The standing-wave laser field in the PBC was crossed by an intense, collimated beam of cesium atoms. The cesium beam was produced in a two-stage oven where the nozzle region was maintained hotter than the main body to reduce the Cs$_2$ dimer fraction. The exit of the oven was a Galileo Electro-optics glass capillary array of 10 μm by 0.05-cm channels with an area of 0.5 cm$\times$2.5 cm. The cesium beam was further collimated in the y direction by passing through a stainless-steel multislit collimator. Several liquid-nitrogen cooled copper plates were placed upstream and downstream of the collimator to pump away cesium and thereby reduce the background cesium pressure. A small amount of background gas still remained, however, showing up as a broad pedestal amounting to a few percent of the transition signal size. At the intersection with the laser beam, the cesium intensity was 10^{15} atoms cm^{-2} s^{-1} with a full angle divergence of 0.04 rad in the y direction.

The laser cesium beam interaction region is shown in more detail in Fig. 5. Not shown in the figure is a 30-cm-diameter Helmholz pair which produced the 70-G magnetic field. The intersection of the beams was a cylinder 0.05 cm in diameter by 2.7-cm long. Two millimeters above and below this line were optically transparent, electrically conductive coated (InSnO$_2$) flat glass plates which had dimensions 2.5 cm$\times$5.0 cm. A dc electric field of ± 2.5 kV/cm was produced by applying a positive or negative voltage to the top plate and grounding the lower plate. As with the polarization (P) reversal, this voltage was reversed using a high-voltage double-pole double-throw vacuum relay. As will be discussed in Sec. IV, the plates were heated to avoid stray electric fields. We supplied $\frac{1}{2}$ W to each plate by running ac (17 kHz) current through the ~ 100-Ω conductive coatings. This
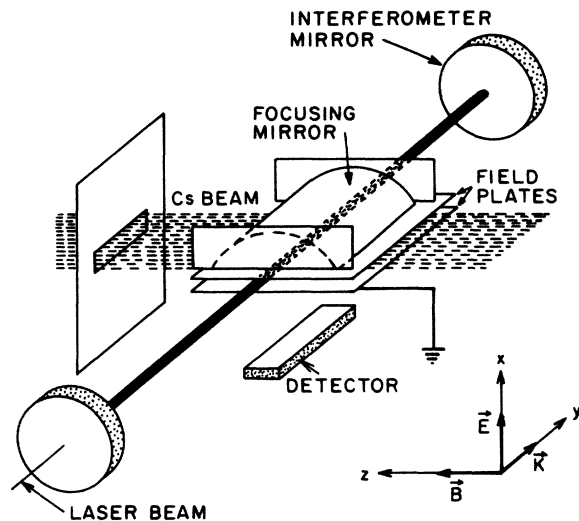
FIG. 5. Detail of the interaction region.

current was sent through isolation transformers to reject any dc component and to isolate the heater supply from the high voltage.

The 850- and 890-nm light from the decay of the 7S state was detected by a liquid-nitrogen cooled rectangular silicon photodiode (active area 0.5$\times$5.6 cm) situated below the lower field plate. A gold-coated cylindrical mirror above the top plate imaged the interaction region onto this detector. Colored glass filters in front of the detector blocked the scattered green laser light while passing the infrared. The output of the photodiode went to a low-noise preamplifier. The detector-preamp combination had a frequency response of ~ 400 Hz ($f_{3\,\mathrm{dB}}$) with a noise equivalent power of 8×10^{-15} W/Hz$^{1/2}$. The signal from the preamp was sent to a gated integrator controlled by a Digital Equipment Corporation PDP11/23 computer which also stored the integrated data. A more detailed discussion of the data acquisition scheme will be given in the following section.

An additional frequency stabilization loop was necessary to remove the effects of thermal drift of the reference cavity. To accomplish this we dithered the laser frequency at 330 Hz by feeding a sine wave to the galvonometer driven Brewster angle plate in the reference cavity. The ~ 2-MHz amplitude of this dither gave rise to a slight modulation on the cesium transition signal. The transition signal, along with the 330-Hz reference, was sent to a lock-in amplifier which provided a very low-frequency correction signal for the reference cavity. We were careful to make sure that this modulation did not produce any signals at the parity reversal frequencies.

B. Data acquisition and analysis

A typical data run consisted of 8 h of data accumulation divided equally between the $F = 4 \rightarrow 3$ and $F = 3 \rightarrow 4$ transitions. For each hyperfine transition, the laser frequency was locked to the extreme high- or low-frequency line of the multiplet shown in Fig. 3(c). A PDP11/23

computer produced the TTL (transistor-transistor logic) signals which controlled the P, E, and B reversals. The reversal rates were 2, 0.2, and 0.02 Hz, respectively, with regular 180° phase shifts introduced in the switching cycles. The transition detector signal was integrated, digitized, and stored for each half cycle of P. Brief deadtimes after each field reversal were necessary to avoid transient effects. The deadtimes used were 25 ms for the P reversal and an entire P cycle (450 ms) for the E and B reversals. After 30 min of data acquisition, the laser was tuned to the other end of the hyperfine multiplet and data acquisition was continued. For normalization purposes, the average signal size was measured using a digital voltmeter and recorded for each data file. The integrator output was also calibrated using this voltmeter. Tests for systematic errors, discussed in the following section, were made before and after each 8 h run.

We analyzed each data file to determine the fraction of the total signal which modulated with the P, E and B reversals. From Eq. (8) this fraction, disregarding systematic effects, is

$$\Delta_{\text{PNC}} = 2(\varepsilon_x/\varepsilon_z)[\text{Im}\mathscr{E}_{\text{PNC}}/(\beta E)] . \tag{10}$$

The m reversal was implemented by subtracting the Δ_{PNC} for the low-frequency line from that obtained for the high-frequency line of the Zeeman multiplet. In our measurements $\varepsilon_x/\varepsilon_z$ was close to 1 and E fields between 1750 and 3000 V/cm were used. With a typical voltage of 2500 V/cm we obtained a detector current of $\sim 3 \times 10^{-10}$ A and a parity nonconserving fraction of $\sim 1.3 \times 10^{-6}$.

IV. CONTRIBUTIONS DUE TO SYSTEMATIC EFFECTS

Systematic errors were of fundamental concern in the design and execution of this experiment. This led to the use of four independent reversals to identify the PNC signal. The quality of each of the reversals was better than one part in 10^4. Thus, in principle, we would only require two reversals to cleanly resolve the PNC signal. The two extra reversals provide redundancy which greatly reduces the potential systematic error, since nearly all of the factors which affect the transition rate are at most correlated with only one reversal. The primary concern then becomes the small imperfections in the various field orientations and field reversals which can give signals that mimic the parity nonconserving signal under every reversal. As discussed below, we have identified and measured all such possible errors. Our approach to the identification of these contributions was similar to that used in earlier Stark interference experiments. Using Eqs. (1) and (3) we derived the transition rate for the general case, allowing for all possible components of $\mathbf{E},\mathbf{B},\boldsymbol{\varepsilon}$, and the oscillating magnetic field $\mathbf{k} \times \boldsymbol{\varepsilon}$. Each of these components was given a reversing and nonreversing part to characterize its behavior under the P, E, B, and m parity reversals. In this analysis, the $\hat{\mathbf{y}}$ axis was taken to be along the laser beam. This means that ε_y is absent by definition. The $\hat{\mathbf{x}}$ axis of the system was defined to be along the component of the applied E field (i.e., the reversing E field) which was perpendicular to the $\hat{\mathbf{y}}$ axis. With this definition, the

$\hat{\mathbf{z}}$ component of the reversing part of E (E_z) is absent but there can be a nonreversing stray field part, ΔE_z. These definitions give the following behavior for the E field upon reversal:

$$E_x\hat{\mathbf{x}} + E_y\hat{\mathbf{y}} \rightarrow (-E_x + \Delta E_x)\hat{\mathbf{x}} + (-E_y + \Delta E_y)\hat{\mathbf{y}} + \Delta E_z\hat{\mathbf{z}} ,$$

$$|E_x| \gg |E_y| \gg |\Delta E_x|, |\Delta E_y|, |\Delta E_z| . \tag{11}$$

The P reversal ($\varepsilon_x \rightarrow -\varepsilon_x$) can be characterized as

$$\varepsilon_z\hat{\mathbf{z}} + i\varepsilon_x\hat{\mathbf{x}} \rightarrow (\varepsilon_z + \delta\varepsilon_z + i\delta\varepsilon_z')\hat{\mathbf{z}} - i(\varepsilon_x + \delta\varepsilon_x + i\delta\varepsilon_x')\hat{\mathbf{x}} ,$$

$$\varepsilon_z \approx \varepsilon_x \gg \delta\varepsilon_{x,z}, \delta\varepsilon_{x,z}' \tag{12}$$

where ε_x and ε_z are real.

We considered all the combinations of these field components which contribute to the $6S \rightarrow 7S$ transition rate. Using rough empirical limits for these components, all terms which could be greater than 0.1% of the true PNC were identified. Effectively, this limit means that we needed only to consider terms which changed sign with all four reversals and involved no more than two components which were either stray or misaligned fields. The three terms which satisfy these criteria, along with their typical values, are listed in Table I. Counterparts of all of these terms were considered in earlier PNC experiments, as discussed in Ref. 13. The first term in the table arises from an electric field misalignment (E_y) and a stray E field (ΔE_z). The second term is due to the stray E field in the y direction (ΔE_y) and a misalignment (B_x) of the magnetic field. The component B_x causes a mixing of states within a particular hyperfine level, and, to a smaller extent mixing of different hyperfine levels with the same principal quantum number. We calculated the size of this mixing using first-order perturbation theory.

The third term in Table I is due to the $A_{\text{ST}} - A_{M1}$ interference shown in Eq. (8). As mentioned previously, this interference is suppressed by its change in sign under reversal of the laser propagation direction, $\hat{\mathbf{k}}$. For our standing-wave field, this suppression factor, relative to the PNC interference, is about 10^3 (PBC output mirror $R \sim 99.8\%$). A second suppression comes from the fact that, though the $M1$ interference mimics the PNC interference under the E, B, and m reversals, it does not change sign under the P reversal. However, imperfections in the P reversal, such as those indicated in Eq. (12), can cause a significant amount of the $M1$ interference to leak

TABLE I. Terms which mimic the PNC signal, given as a ratio to the pure Stark induced transition rate of Eq. (8).

Term	Average size relative to PNC term
1 $\dfrac{E_y \Delta E_z}{E_x^2} \dfrac{\varepsilon_x}{\varepsilon_z}$	0.01
2 $\dfrac{\Delta E_y}{E_x} \dfrac{B_x}{B_z} \dfrac{\varepsilon_x}{\varepsilon_z}$	0.04
3 $\sqrt{2} \left[\dfrac{\delta\varepsilon_z^{k+} - \delta\varepsilon_z^{k-}}{|\varepsilon_z|} \right] \dfrac{M}{\beta E_x}$	0.17

through since $M/(\text{Im}\mathscr{E}_{\text{PNC}})\sim 10^4$. Of particular concern is the birefringence in the power-buildup-cavity output-mirror coating as discussed in Ref. 14. This can give rise to an asymmetry between the fields of the counterpropagating laser beams which changes sign with the P reversal. There is an additional contribution to this term which involves the birefringence of the input mirror and other optics. However, these birefringences also cause a modulation in the transition signal size when the polarization is reversed which is about 10^5 times larger than the PNC systematic. We observed this modulation and added birefringence to cancel it. With this cancellation the PNC systematic involving these birefringences is negligible leaving only that due to the output mirror. For a more detailed discussion of this point see Ref. 14 or Ref. 15.

We have designed a set of auxiliary experiments to measure the fields which contribute to terms 1–3 in Table I. Our basic philosophy was that we should be able to monitor all the possible systematics while we were taking PNC data. To do this we used the atoms themselves to measure the fields which give rise to the three terms in Table I. This was done without changing the basic experimental configuration. As can be seen below, the procedures used were somewhat excessive for the level of precision of the present measurement. However, much of this effort was preparation for the more precise measurements we plan to make using this technique. The following is a description of each of these auxiliary experiments.

(a) $\Delta E_z/E_x$ measurement. Conditions: linearly polarized laser light $\boldsymbol{\varepsilon}=\varepsilon_x\hat{\mathbf{x}}+\varepsilon_z\hat{\mathbf{z}}$; $|\mathbf{B}|=0$. The $F=4\rightarrow4$ Stark-induced transition rate from Eq. (1) is given by

$$I_4^4 = 9\alpha^2(\mathbf{E}\cdot\boldsymbol{\varepsilon})^2 + \tfrac{15}{4}\beta^2\,|\,\mathbf{E}\times\boldsymbol{\varepsilon}\,|^2$$

$$\approx 9\alpha^2(E_x^2\varepsilon_x^2 + 2E_xE_z\varepsilon_x\varepsilon_z) \tag{13}$$

since $\alpha/\beta\approx10$ and $E_x\gg E_y,E_z$. The modulation (amplitude) of this transition rate with the E reversal is

$$[\Delta I_4^4]_E \approx 9\alpha^2(E_x\Delta E_x\varepsilon_x^2 + E_x\Delta E_z\varepsilon_x\varepsilon_z)\;. \tag{14}$$

The above measurement was made and the laser polarization was then rotated to $\boldsymbol{\varepsilon}'=\varepsilon_x\hat{\mathbf{x}}-\varepsilon_z\hat{\mathbf{z}}$. This causes the second term in Eq. (14) to change sign. The difference between these two measurements, divided by the overall transition rate yields

$$\frac{[\Delta I_4^4(\varepsilon)]_E - [\Delta I_4^4(\varepsilon')]_E}{\overline{I}_4^4} = 2\frac{\Delta E_z}{E_x}\frac{\varepsilon_z}{\varepsilon_x}\;. \tag{15}$$

Knowing $\varepsilon_x/\varepsilon_z=1.0$, we obtained $\Delta E_z/E_x$.

(b) E_y/E_x measurement. Conditions: circularly polarized light $(\boldsymbol{\varepsilon}=\varepsilon_z\hat{\mathbf{z}}+i\varepsilon_x\hat{\mathbf{x}})$; $B_z=70$ G; an additional magnetic field in the $\hat{\mathbf{x}}$ direction, $B_x'=0.15B_z$. In this measurement we monitored the transition rate on the two outermost lines for both the $F=4\rightarrow3$ and $F=3\rightarrow4$ Zeeman multiplets. The effect of the additional magnetic field, B_x', is the replacement of B_x with $(B_x+B_{x'})$ in term 2 of Table I. The fractional modulation of the transition rate with the P, B_x', and m reversals is then

$$\frac{(\Delta I_{4m}^{3m'})_{P,B_x',m}}{I_{4m}^{3m'}} = 2\frac{E_y}{E_x}\frac{B_x'}{B_z}\frac{\varepsilon_x}{\varepsilon_z}\;. \tag{16}$$

The fields B_z and B_x' were measured using a gaussmeter and again $\varepsilon_x/\varepsilon_z=1$. With this information and the measurement represented by Eq. (16), we solved for E_y/E_x.

(c) $\Delta E_y/E_x$ measurement. Conditions: same as in (b). The measurement is identical to that outlined in (b) with the addition of the E reversal

$$\frac{(\Delta I_{4m}^{3m'})_{P,E,B_x',m}}{I_{4m}^{3m'}} = \frac{\Delta E_y}{E_x}\frac{B_x'}{B_z}\frac{\varepsilon_x}{\varepsilon_z}\;. \tag{17}$$

This measurement was made simultaneously with measurement (b) and the stored data were analyzed to obtain E_y/E_x and $\Delta E_y/E_x$.

(d) B_x/B_z measurement. Conditions: same as in (b) but with $B_x'=0$. These were the same conditions as used in the PNC measurement. The fractional modulation of the transition rate with the P, B, and m reversals is

$$\frac{(\Delta I_{4m}^{3m'})_{P,B,m}}{I_{4m}^{3m'}} = 2\frac{E_y}{E_x}\frac{B_x}{B_z}\frac{\varepsilon_x}{\varepsilon_z}\;. \tag{18}$$

This measurement takes no additional time as it was derived from the raw parity nonconservation data. The desired quantity, B_x/B_z, was obtained from Eq. (18) since E_y/E_x was known from (b) and $\varepsilon_x/\varepsilon_z$ was measured for each data run.

(e) $(\delta\varepsilon_z^{k^+} - \delta\varepsilon_z^{k^-})$ measurement. Conditions: circular laser polarization; $|\mathbf{B}|=0$; cesium-beam collimator tilted such that the Cs beam is no longer perpendicular to the laser beam. In this situation, it is simplest to think of the power-buildup-cavity laser field as being made up of two superimposed traveling waves with opposite propagation vectors, $\hat{\mathbf{k}}^+=+\hat{\mathbf{y}}$ and $\hat{\mathbf{k}}^-=-\hat{\mathbf{y}}$. Due to the tilted collimator, a particular cesium transition is now split into two peaks; one corresponding to the Doppler-shifted resonance with $\hat{\mathbf{k}}^+$ component of the laser field, and the second corresponding to the Doppler-shifted resonance with the $\hat{\mathbf{k}}^-$ component. Using this method we were able to clearly resolve these peaks, as shown in Fig. 6. For the $F=4\rightarrow3$ transition, the transition rates for these two peaks are

$$I_4^3(k^+)=\tfrac{21}{4}\beta^2E_x^2\,|\,\varepsilon_z^{k^+}\,|^2,\quad I_4^3(k^-)=\tfrac{21}{4}\beta^2E_x^2\,|\,\varepsilon_z^{k^-}\,|^2\;.$$

$$\tag{19}$$
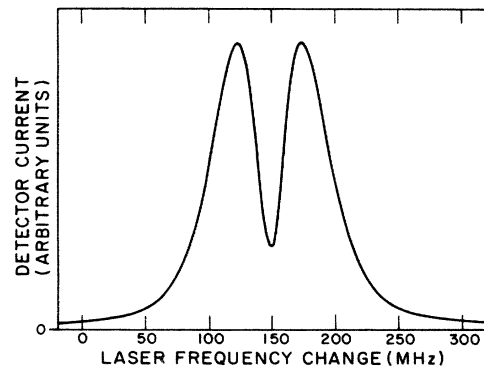
FIG. 6. Scan of the $6S_{F=4}\rightarrow7S_{F=4}$ transition with the cesium-beam collimator tilted so that the $\hat{\mathbf{k}}^+$ and $\hat{\mathbf{k}}^-$ peaks are resolved $(B=0$ G$)$.

The difference in fractional modulation with the P reversal for the two peaks is then

$$\frac{[\Delta I_4^3(k^+)]_p}{I_4^3(k^+)} - \frac{[\Delta I_4^3(k^-)]_p}{I_4^3(k^-)} = \sqrt{2}\left|\frac{\delta\epsilon_z^{k^+} - \delta\epsilon_z^{k^-}}{|\epsilon_z|}\right|,$$

(20)

where we have used $|\epsilon_z^{k^+}| \approx |\epsilon_z^{k^-}| \approx (1/\sqrt{2})|\epsilon_z|$. The expression in Eq. (20) is identical to the coefficient of $M/(\beta E_x)$ in term 3 of Table I. The ratio $M/(\beta E)$ has been measured previously.[16]

Measurements (a), (b), and (c) were made at the beginning and end of each data run to guard against the possibility of ΔE_y and ΔE_z changing with time. These measurements took about 1 h to complete and, when combined with measurement (d), resulted in an uncertainty for terms 1 and 2 in Table I which was typically an order of magnitude smaller than the statistical uncertainty in the PNC measurement. As discussed below, measurement (e) was only made if the PBC output mirror had been moved or rotated.

A number of additional tests were made to verify that these field imperfections gave the false signals predicted by Table I, both in magnitude and sign. In each test, a particular term was enhanced and the systematic tests (a)—(e) were made. Parity nonconservation data were then taken and the predictions of the systematic tests were compared with the measured false PNC signals. Nonreversing E fields ΔE_y and ΔE_z of 3 volts/cm ($\Delta E_{y,z}/E_x \sim 10^{-3}$) were produced by applying dc voltages across each field plate. The large reversing B_x field ($B_x/B_z = 3\times10^{-2}$) was produced with an external coil that was reversed with the B_z coil. A mirror with a large coating birefringence was put into the PBC to enhance term 3 in Table I. For each of these tests, the prediction of the systematic tests agreed with the measured false PNC to within the uncertainties of the measurements (10—20%).

We have carried out extensive studies of the effects which give rise to the terms of Table I. These studies achieved two goals: they led to modifications in the apparatus which reduced the size of the necessary corrections, and reduced the time variation of the systematic errors. This latter point is by far the most important. The measurements described above allow us to measure all the corrections to a high degree of accuracy relative to the PNC rate in a short time. This means it is not particularly important how big these corrections are but it is crucial to know if they vary during the time we then spend taking PNC data. We found that the stray electric fields in particular could be highly time dependent and quite large if preventative measures were not taken. Especially troublesome was the fact that every material we tested tended to acquire stray electric fields after it was exposed to the cesium beam for some time. We tried many different kinds of field plates before arriving at the heated conductive coatings we presently use. Purely empirically we have determined that if these field plates are kept somewhat above room temperature (but not too far above) they have

very desirable characteristics. When first put into the apparatus they had some modest initial $\hat{y}$ and $\hat{z}$ stray fields, perhaps 0.25 V/cm. After brief exposure to the cesium beam the stray fields would drop to less than 0.05 V/cm; one to two parts in 10^5 of the total applied E field. We saw only very slow subsequent drifts in these stray fields.

The misaligned fields (E_y and B_x) were quite stable as expected since all the components of the apparatus were rigidly mounted. The E_y field depends on the alignment of the electric field plates with the laser beam. We found that we could set this alignment to make $E_y/E_z = 10^{-4}$. However, a nominal alignment of $E_y/E_x \simeq 10^{-3}$ was used as a compromise between enhancing the signal for measurement (d) and minimizing term 1 in Table I.

Magnetic field coils in the $\hat{x}$, $\hat{y}$, and $\hat{z}$ directions were used to shim out stray (nonreversing) and misaligned (reversing) B fields. Although most of these fields do not produce false PNC signals, they can give rise to signal modulations with the P reversal which complicated the systematic tests. Thus we found it worthwhile to eliminate them. The appropriate nonreversing shim field settings were determined by measuring these fields with a gaussmeter. These fields were reduced to about 10 mG. The reversing field shims were set by monitoring the signal modulation with the P, B, and m reversals. After this adjustment, B_x/B_z was typically 3×10^{-3}.

The possibility of E and B field inhomogeneity along the 1-in line of intersection of the cesium and laser beams was also investigated. The measurements (a)—(d) are only sensitive to the average value of the quantities $\Delta E_y/E_x$, $\Delta E_z/E_x$, E_y/E_x, and B_x/B_z. These average values were then combined to calculate terms 1 and 2 in Table I. This approach is not strictly correct, however, if both components which make up a single term have spatial inhomogeneity. We tested for this possibility by taking measurements (a)—(d) under the normal conditions and then repeated them with about half the length of the cesium beam blocked. As we expected, these data showed that there were indeed spatial variations in the stray E fields (ΔE_y and ΔE_z) of roughly 50%. However, E_y and B_x were found to be homogeneous to better than 10%. This confirms that there is only one inhomogeneous field in each of the terms, and therefore our measurements are valid.

The corrections we measure before and after each data run support the conclusion that the stray electric fields vary little with time. The second term in Table I was always found to be the same before and after to within the statistical uncertainty. The average size of this correction for a data run was 3.5% of the PNC with an uncertainty of about the same size. The first term varied by more than the statistical uncertainty on about half the runs. This was hardly grounds for concern, however, since the average value for this correction was 0.4% of the PNC and the typical statistical uncertainty was half of that. When there was variation, we used the average of the two corrections. The error bars were then taken to cover both values, which at worst differed by 0.4% of the PNC. Since the statistical uncertainty in the PNC measurement was about 20% for each data run it is clear that it was not really necessary to check the stray fields before and after

each run. Our previous experience, however, made us wary of relying on their constancy until a considerable amount of supporting evidence had been obtained.

The only apparatus dependence to term 3 of Table I is the coating birefringence of the PBC output mirror, or to be more precise, the product of the coating birefringence times the angle between the birefringence axis and the x axis. Measurement (e) listed above is a very sensitive way to determine the actual correction due to this term. However, we found the following procedure was a simpler way to study the general characteristics of the birefringence. With the vacuum chamber up to air, the transmission through a linear polarizer following the PBC was monitored while the circular polarization of the laser was reversed. The modulation of this signal showed a periodic dependence with the rotation of the output mirror (PBC on resonance), due to the combination of the output mirror coating and substrate birefringences. The generally smaller contribution due to the substrate birefringence was determined by the same procedure but with the input mirror removed. Using this approach the axis and amount of the output-mirror coating birefringence could be determined. We investigated a number of mirrors from different manufacturers in this manner. In agreement with Ref. 14 we found that the coating birefringence was a general property which varied from mirror to mirror, but for a particular mirror it was largely the same across the entire surface. We did find that there were occasional, usually very local, regions where the birefringence could be significantly different, however. This is in contrast to the results reported in Ref. 14 but we believe this is because the method used in that reference was insensitive to local variations. Based on a limited number of test samples we now believe the birefringence is predominantly determined by the geometry of the coating facilities when the mirror is made. We saw no temporal variations in the coating birefringence.

Before taking PNC data we rotated the output mirror to reduce term 3 in Table I. If the angle between the birefringence axis and the x axis is zero, this term vanishes. Because of the spatial variation in the coating and the substrate we could only set this angle to within a few degrees, however. The residual birefringence correction to the PNC data was then determined as described in measurement (e). Because earlier tests had shown there was no time variation to this correction term, measurement (e) was repeated only if the mirror was moved or the laser alignment was changed. We found that laser alignment had very little effect, but rotation of the mirror made a substantial difference, as shown below.

For about one third of the data the correction due to term 3 was $+49(4)\%$ of the PNC, for the second third it was $-58(4)\%$, and for the remainder it was $-0.4(1.0)\%$. Although these corrections are relatively large, they can be accurately determined and hence are not a serious problem here. However, we have now obtained mirrors with far lower birefringence which will be used in future work.

Another conceivable systematic effect we considered was one due to a dependence of the detector sensitivity on the direction of **E** and/or **B**. We tested for this effect by monitoring the detector signal while reversing both **E** and **B**. A stable light level was provided by a light-emitting diode. We found that there was no change in detector sensitivity at the part in 10^5 level. The existence of the other reversals makes any residual effect from this source negligible. We have also considered the effects of motional **E** and **B** fields which arise because the atoms are moving through magnetic and electric fields and we also find these to be negligible.

We believe that there are no significant contributions that mimic the PNC signal which have not been taken into account. It should be noted that the uncertainty in determining these corrections is predominantly statistical. Thus improved signal to noise will not only reduce the statistical uncertainty on the PNC results but will also reduce the uncertainty in the corrections.

The only remaining source of systematic error is in the calibration of the experiment. This calibration involves measuring the dc electric field, the ratio $\varepsilon_x/\varepsilon_z$, and determining the contributions to the observed detector current which are not represented in Eq. (9). Such contributions have often been called "dilutions" in earlier papers on this subject. The electric field was determined from the applied voltage and the measurement of the separation of the field plates. The 0.5% uncertainty to this calibration came entirely from the separation measurement. We have previously shown that more accurate field measurements can be made by observing the Stark shift of the cesium atoms, but that was unnecessary for this experiment. We determined $\varepsilon_x/\varepsilon_z$ by measuring the polarization of the light which was transmitted by the power-buildup cavity using a linear polarizer and a photodiode.

To measure the background signals we periodically set the static electric field to zero and observed the detector current. This was then subtracted off the signal observed with the **E** field on. The principal source of background was laser induced fluorescence of the optics which was typically 0.15 times the cesium signal. Though this background did not introduce any systematic uncertainty, it did increase the overall noise by about a factor of 2 and thus increased the statistical uncertainty in our results. The only additional background we observed came from cesium molecules and was about a factor of 5 smaller. We tested for any **E** field dependent background by tuning the laser frequency well off the transition and measuring the signal for **E** on and off. This set an upper limit of 10^{-4} times the atomic transition signal for such background.

A small calibration correction was needed because of the incomplete resolution of the lines in the Zeeman multiplet, as seen in the experimental spectrum of Fig. 3. This correction was obtained in the following way. First, we scanned the laser to obtain the transition spectra for both $|\mathbf{B}|=0$ G and $|\mathbf{B}|=70$ G. The 70 G spectrum, such as that shown in Fig. 3(c), was then fitted as the sum of eight individual lines where each line was assumed to have the 0 G line shape. From this fit we found the contribution of the overlapping lines and, using Eq. (9) we calculated the appropriate correction. This was done for each data run and the correction was typically 4% with negligible uncertainty.

V. RESULTS AND CONCLUSIONS

Ten data runs were made in the manner described in Sec. III. The signal-to-noise ratio was typically two or three times worse than that expected in the shot noise limited case. This extra noise was due primarily to the scattered-light-induced fluorescence background mentioned previously. This resulted in an integration time of 20—30 min for a 100% measurement of the PNC term. Our combined results for the ten data runs are

$$
\text{Im}\mathscr{E}_{\text{PNC}}/\beta = \begin{cases} -1.51\pm0.18 \text{ mV/cm} \quad (F=4\to3)\,, \\ -1.80\pm0.19 \text{ mV/cm} \quad (F=3\to4)\,, \\ -1.65\pm0.13 \text{ mV/cm} \quad (\text{average})\,, \end{cases}
$$

where the quoted uncertainty includes all sources of error. As discussed earlier, the uncertainty is dominated by the purely statistical contribution. Our value is in good agreement with the value of $-1.56\pm0.17\pm0.12$ mV/cm reported by Bouchiat *et al.* for the average of measurements made on the $F=4\to4$ and $3\to4$ hyperfine transitions.[5]

Using $\beta=27.3(4)a_0^3$ as discussed in Appendix B, we obtain

$$
\text{Im}\mathscr{E}_{\text{PNC}} = -0.88(7)\times10^{-11}ea_0\,.
$$

To relate this to the weak charge Q_w, or equivalently $\sin^2\theta_w$, it is necessary to know the value of the matrix element in Eq. (6). As we mentioned in Ref. 6 there is some uncertainty in the theoretical evaluation of this quantity. The most extensive calculation has been carried out by Dzuba *et al.*[17] and their result of $\mathscr{E}_{\text{PNC}}=0.88(3)\times10^{-11}iea_0(Q_w/N)$ is probably the best value to take for this quantity and its uncertainty. However, a very conservative view would allow a range from 0.85 to 0.97 as can be seen in Ref. 18. It is likely that new results will be forthcoming in the near future which will clarify and hopefully improve this situation. Using the value of Ref. 17 our experimental results give

$$
Q_w = -78\pm6\pm3
$$

for the cesium experiment. Where the first uncertainty is due to our experimental uncertainty and the second is due to the theoretical uncertainty. This is in good agreement with the standard model value[17] using $\sin^2\theta_w$ obtained from the mass of the W boson,

$$
Q_w = -71.0\pm1.7\pm3.0
$$

for the standard model prediction. The experimental value of Q_w can also be used to obtain the weak mixing angle. Using the renormalized weak charges[1] for the proton and neutron this gives

$$
\sin^2\theta_w = 0.257\pm0.028\pm0.014
$$

for the cesium experiment.

A comparison of the PNC measurements for the two hyperfine lines provides information on the nucleon spin-dependent coupling constants. Novikov *et al.*[19] have calculated the difference in the PNC between the $F=4\to3$ and $3\to4$ lines using a shell model for the nucleus. They find that the difference is the flip of one proton spin with an estimated uncertainty of 30%. Using this result and our measurements of the two hyperfine lines we find

$$
C_{2p} = -2\pm2
$$

where C_{2p} is the proton-axial-vector—electron-vector neutral-current coupling constant. This is in agreement with the predicted value of 0.1 and is a substantial improvement over the previous experimental limit of $C_{2p}<100$ (Ref. 5).

The agreement between our measurements and the predictions of the standard model has implications for a variety of alternative models. It limits the possible values for masses of additional bosons and the strengths of coupling constants in superstring theories,[20] supersymmetric theories,[21] and others. However, a discussion of this topic is beyond the scope of this paper.

VI. FUTURE

We believe the experimental technique we have presented here is still in a rather youthful state and that future measurements will provide substantially higher precision. The systematic uncertainties do not appear to be a limitation until a precision of parts in 10^3 of the PNC is reached. Thus the primary question, which we are actively exploring, is how much the statistical uncertainty can be improved. It is already clear that significant improvements can be achieved with better optics which will provide less scattered light and higher standing-wave fields in the PBC. Another obvious improvement is the use of a spin-polarized cesium beam. Presently only $\frac{1}{16}$ of all the cesium atoms are in the spin state which we exite. We have developed[22] a diode laser optically pumped cesium beam which has essentially all the atoms in a single spin state and so will provide much larger PNC signals. With these improvements we believe that the PNC interaction in cesium will be measured to well under 1% as this technique matures. Precise measurements in rubidium will also be possible using the same approach. These data will be a major contribution to our understanding of the neutral-current interaction.

APPENDIX A: $C_{Fm'}^{F'm'}$ COEFFICIENTS

The coefficients $C_{Fm}^{F'm'}$ are proportional to the usual Clebsch-Gordon coefficients and are tabulated in the following:

$$
C_{4,m'}^{4,m'} = +\frac{m'}{4}\,,
$$

$$
C_{4,m'-1}^{4,m'} = -\tfrac{1}{8}[(5-m')(4+m')]^{1/2}\,,
$$

$$
C_{4,m'+1}^{4,m'} = +\tfrac{1}{8}[(5+m')(4-m')]^{1/2}\,,
$$

$$C^{3,m'}_{4,m'} = \frac{+(16-m'^2)^{1/2}}{4} \ ,$$

$$C^{3,m'}_{4,m'-1} = -\tfrac{1}{8}[(4-m')(5-m')]^{1/2} \ ,$$

$$C^{3,m'}_{4,m'+1} = -\tfrac{1}{8}[(4+m')(5+m')]^{1/2} \ ,$$

$$C^{4,m'}_{3,m'} = \frac{+(16-m'^2)^{1/2}}{4} \ ,$$

$$C^{4,m'}_{3,m'-1} = +\tfrac{1}{8}[(3+m')(4+m')]^{1/2} \ ,$$

$$C^{4,m'}_{3,m'+1} = +\tfrac{1}{8}[(3-m')(4-m')]^{1/2} \ ,$$

$$C^{3,m'}_{3,m'} = -\frac{m'}{4} \ ,$$

$$C^{3,m'}_{3,m'-1} = +\tfrac{1}{8}[(4-m')(3+m')]^{1/2} \ ,$$

$$C^{3,m'}_{3,m'+1} = -\tfrac{1}{8}[(4+m')(3-m')]^{1/2} \ .$$

APPENDIX B: THE VALUE OF β

The tensor transition polarizability, β, is found by combining several experimental and theoretical results as first discussed in Ref. 23. The value which has been quoted in the literature has varied slightly with time as new inputs

for these quantities have become available. We take β to be $27.3(4)a_0^3$. The experimental inputs which we use to obtain this number are the ratio $\alpha/\beta = -9.9(1)$ from Refs. 24–26, the $7S$ state lifetime from Ref. 27, the $7S$ state polarizability from Ref. 28, the oscillator strengths f_{66} and f_{76} from Ref. 29, and the measured energy differences of the states involved. As discussed in Ref. 28, the primary theoretical input is the calculation of the contribution to α from the states with principal quantum numbers greater than or equal to 8. From the recent work of Johnson and co-workers[30] we take this to be $\Delta\alpha = -4.5(6)a_0^3$.

The value of β we give here differs from our previously quoted value of $26.6(4)a_0^3$ primarily because of a change in the measured value of the $7S$ lifetime. Here we are using the newer more precise value obtained by Bouchiat et al.[27] instead of the value from Ref. 23 which we had used earlier. Our present value of β is also slightly different from the value of $26.8(5)a_0^3$ first given in Ref. 27 and repeated in many subsequent publications by the same group (in some of the later references the uncertainty was increased from 5 to 8). The $26.8a_0^3$ result was obtained by using the value of $\Delta\alpha$ calculated in Ref. 31. As discussed in Ref. 30, that value for $\Delta\alpha$ is incorrect.

*Present address: Time and Frequency Division, National Bureau of Standards, Boulder, CO 80303.

[1]W. J. Marciano and A. Sirlin, Phys. Rev. D 27, 552 (1983).

[2]H. Hollister et al., Phys. Rev. Lett. 46, 643 (1981), and references therein.

[3]T. P. Emmons, J. M. Reeves, and E. N. Fortson, Phys. Rev. Lett. 51, 2089 (1983).

[4]P. H. Bucksbaum, E. D. Commins, and L. R. Hunter, Phys. Rev. D 24, 1134 (1981); P. S. Drell and E. D. Commins, Phys. Rev. Lett. 53, 968 (1984).

[5]M. A. Bouchiat, J. Guena, L. Hunter, and L. Pottier, Phys. Lett. 117B, 358 (1982); 134B, 463 (1984).

[6]S. L. Gilbert, M. C. Noecker, R. N. Watts, and C. E. Wieman, Phys. Rev. Lett. 55, 2680 (1985).

[7]M. A. Bouchiat and C. Bouchiat, J. Phys. (Paris) 35, 899 (1974); 36, 493 (1975).

[8]A somewhat different method using high magnetic fields (~ 1 kG) in cell experiments was proposed independently by M. A. Bouchiat, M. Poirier, and C. Bouchiat, J. Phys. (Paris) 40, 1127 (1979); and by E. Commins [see P. H. Bucksbaum, in Proceedings of the Workshop on Parity Violation in Atoms, Cargèse, Corsica, 1979 (unpublished)]. This method was used in the 1984 thallium measurement (Ref. 4).

[9]See Ref. 8, M. A. Bouchiat et al.

[10]Another field configuration is possible using linearly polarized laser light. This configuration was used in the 1984 thallium measurement (Drell and Commins, Ref. 4). For our particular experiment, the advantages and disadvantages of these two field configurations are discussed in Ref. 15.

[11]T. W. Hänsch and B. Couillaud, Opt. Commun. 35, 441 (1980).

[12]R. W. P. Drever, J. L. Hall, F. V. Kowalski, J. Hough, G. M. Ford, and A. J. Munley, Appl. Phys. B 31, 97 (1983).

[13]P. S. Drell and E. D. Commins, Phys. Rev. A 32, 2196 (1985).

[14]M. A. Bouchiat, A. Coblentz, J. Guena, and L. Pottier, J. Phys. (Paris) 42, 985 (1981).

[15]S. L. Gilbert, Ph.D. thesis, University of Michigan, 1984 (unpublished).

[16]S. L. Gilbert, R. N. Watts, and C. E. Wieman, Phys. Rev. A 29, 137 (1984). The $M1$ amplitude, M, has a slight dependence on F and F'. This has been taken into account in our adjustments due to the $M1$ systematic error.

[17]V. A. Dzuba, V. V. Flambaum, P. G. Silvestrov, and O. P. Sushkov, J. Phys. B 18, 597 (1985).

[18]W. R. Johnson, D. S. Guo, M. Idrees, and J. Sapirstein, Phys. Rev. A 34, 1043 (1986).

[19]V. N. Novikov, O. P. Sushkov, V. V. Flambaum, and I. B. Khriplovich, Zh. Eksp. Teor. Fiz. 73, 802 (1977) [Sov. Phys.—JETP 46, 420 (1977)]. It has been pointed out to us that these data could also be used to provide a limit on the size of the nuclear anapole moment, as discussed by V. V. Flambaum, I. B. Khriplovich, and O. P. Sushkov, Phys. Lett. B 146, 367 (1984).

[20]V. Barger, N. W. Deshpande, and K. Whisnant, Phys. Rev. Lett. 56, 30 (1986).

[21]P. Fayet, Phys. Lett. 96B, 83 (1980).

[22]R. N. Watts and C. E. Wieman, Opt. Commun. 57, 45 (1986).

[23]J. Hoffnagle, V. L. Telegdi, and A. Weis, Phys. Lett. 86A, 457 (1981); J. Hoffnagle, Ph.D. thesis, Swiss Federal Institute of Technology, Zurich, 1982 (unpublished).

[24]J. Hoffnagle, L. Ph. Roesch, V. Teledgi, A. Weis, and A. Zehnder, Phys. Lett. 85A, 143 (1981).

[25]S. L. Gilbert, R. N. Watts, and C. E. Wieman, Phys. Rev. A 27, 581 (1983).

[26]M. A. Bouchiat, J. Guena, L. Hunter, and L. Pottier, Opt. Commun. 45, 35 (1983).

[27]M. A. Bouchiat, J. Guena, and L. Pottier, J. Phys. Lett. (Paris) 45, L523 (1984).

[28]R. N. Watts, S. L. Gilbert, and C. E. Wieman, Phys. Rev. A 27, 2769 (1983).

[29]L. N. Shabanova et al., Opt. Spektrosk. 47, 3 (1979) [Opt.

Spectrosc. (U.S.S.R.) 47, 1 (1979)].

[30]W. R. Johnson et al. (unpublished).

[31]C. Bouchiat and C. A. Piketty, Phys. Lett. B 128, 73 (1983).